Chapter 3

Mathematical Modeling and Simulation

3.1 Introduction

Neurons are the building blocks of intelligence in all living beings, and they're responsible for complicated behaviors like recognition, memory, cognition, etc. Intelligent responses can be observed locally in terms of local feedback circuits or globally in terms of reflex and cognitive reactions. Local muscular contraction in response to a pain trigger is an example of a local feedback response in which the local feedback circuit attempts to avoid discomfort by retracting the trigger point. Similarly, reaction or cognition can be demonstrated by catching or blocking a ball thrown toward a subject. Information is sent to either the central nervous system or the local feedback system, which recognizes it and responds appropriately. The nervous system is responsible for acquiring such information and translating it into appropriate responses, with neurons serving as the primary component responsible for carrying the signal to the central/ peripheral nervous system and generating local or global responses depending on the strength of the stimulus. The general working mechanism of a robust neuronal network in facilitating intelligent responses to incoming information has been argued and discussed for a long time as a progressive learning method, where progressive learning is achieved as a function of inter-network and intra-network weighted connectivity and biases. Raman y Cajal, equipped with Golgi's staining technique and an achromatic microscope, generated vastly detailed drawings of neural circuits, covering several species and most important parts of the brain, in 1888 and advocated the neuron doctrine. Cajal provides the fascinating theory of principles of dynamic polarization and

the physiological characterization of neurons as information processing units in his neuron doctrine. Cajal described the neuron structure into three parts: soma (cell body), dendrites, and axons. Even though neuron doctrine clarifies the concept of neuronal structures, their non-continuous connectivity with the neuronal grid, and the electrical signaling hypothesis, the HH model of excitable neuron membrane published in 1952 provides a mathematical representation of action potential initiation and propagation and helps to understand processes associated with neuronal signaling. AIC dynamics, such as sodium ion channel, potassium ion channel, and leakage ion channel dynamics, have been thoroughly discussed, adding knowledge of active membrane dynamics. The mathematical model proposed by Alan Hodgkin and Andrew Huxley serves as the foundation for recent advancements in modern membrane dynamics, such as Hyper-polarized current, calcium ion signaling, and other recent advancements in contemporary membrane dynamics. Several modified neural models (such as the FitzHugh-Nagumo model and Rall's cylinder model) were also established, allowing for efficient large-scale simulation of populations of neurons and mathematical understanding of action potential firing mechanisms. In contrast to the basic operating mechanism of neurons and neuronal networks, the functional component of a single neuron has received very little attention. Neurons are renowned for having identical morphology, morphogenesis, complex dendritic arborization, and the ability to trigger localized spikes, whereas in-silico models ignore the dendritic arbor's distinctive qualities, portraying dendrite fibers as passive cables exclusively responsible for signal propagation. The dynamic characteristics of dendritic arbors, including localized spiking activity, structure-function relationships, inter-fiber coupling, and their potential role in creating complex neuronal responses, has been confirmed in-vitro. As a result, thorough research of the fundamental components of neuron morphology is urgently required, as is determining the functional significance of such faculties in defining neuronal system dynamics. The involvement of the dendritic arbor and neuronal fibers has been investigated in this study. To comprehend the local dynamics of single fiber as well as bundled neural fiber systems, a mathematical model derived from the infamous "cable equation" has been used. Specific membrane properties from in-vitro and in-silico models are used to simulate local neuronal dynamics. The following sections of this chapter will go through the cable model and observe how to use it to simulate different aspects of the neural fiber.

3.2 Approach

The problem in this chapter is to mathematically model and simulate active and passive fiber dynamics highlighting electrophysiological and morphological attributes of single nerve fiber and bundled nerve fiber systems. Equivalent electrical circuits representing active and passive nerve membrane is used to derive the current and voltage equations that are used to model and simulate neuronal fiber dynamics corresponding to spike generation in active membrane, signal propagation, decremental conduction and inter-fiber interferance in passive membranes. Active membrane model is simulated incorporating electrically equivalent voltage dependent variable resistors for Na^+ and K^+ ions and similarly linear electrical components (resistances and capacitances) in passive membrane as defined in literature. Computation of overall electrical behavior is modeled by taking the length, diameter, membrane surface area and internal volume of the fiber into computational consideration for calculating the cumulative axial and transmembrane conductivity and membrane leakage parameters. Later in the chapter, the concepts of signal propagation, decremntal conduction and transmembrane ionic leakage has been extended to further analyse and simulate their roles in multifibre systems.

3.2.1 Contribution

The proposed work has made a significant contribution to understanding of neuron fiber dynamics and the role of electrophysiological and morphological factors in shaping robust neuronal responses. The simulation model reveals new insights into the effects of various morphology features on nerve signal propagation. Apart from signal propagation dynamics, the cell-field interaction model in bundled nerve fiber provides a detailed understanding of the potential role of bundled fiber coupling in complex function formations like interference-free transmission and correlation detection and tuning.

3.3 Cable Theory and The Cable Model

The application of classical cable theory to study signal propagation dates back to the 1850s when it was used to mathematically model signal attenuation in telegraph cables. The cable equation originates from Fourier's heat conduction

equation, and after focusing on analogies with the heat equation and the telegrapher's equation, Cole and Hodgkin [39, 148], developed the cable equation to mathematically model theories and concepts of conduction in neuronal fiber. The cable equation is a notable development in the field of computational neuroscience for modeling and simulation of nerve structures. The cable equation provides useful information for modeling the electrical and geometric properties of excitable cells. The shape of a neuronal cell, in particular, and the extent of branching in dendrites in general, are key components that contribute to passive responses caused by injected current (from a natural synapse or artificial current source). Simultaneously, the shape and size of the dendrites influence the change in excitable neuronal responses. Cable characteristics are critical in order to mimic complicated neuronal morphologies such as dendrites, soma, and axon.

The cable equation has been used by Goldstein [149], and Rall [47, 150] to represent the change in action potential form and propagation velocity owing to changes in cable geometry. Rall's 3/2 rule and Rall's equivalent cylinder is one of the important findings of this model. In terms of geometric ratios, it also represents the blocking condition for propagating action potential. Rinzel [151] later used Rall's equivalent cylinder to describe transient activity in the neural dendritic tree. Rall's 3/2 rule has been widely applied to dendritic bifurcation modeling. Furthermore, the Agmon-Snir [152] extension of Rall's cable theory, and the Ramon [153] cable model combined with the voltage-clamped approach has implications in modeling the axonal section and passive dendrites, accordingly. For arbitrarily branched cable, the Abbot [154], and Guy Major [155] model offers valuable perspective into efficient signal propagation/reconstruction and coupling of dendritic branches with respect to the growth in their series resistance. Monai [156] uses the cable equation to demonstrate the frequency dependence of a passive shunt dendritic cylinder, and Sweilam [157] model finds its inference in modeling the responses of the dendritic spine head, indicating the significance of the cable equation remedy and its potential ramifications in modeling a diverse range of neuronal morphologies.

Shown in Figure3-1a is the cable equivalent circuit of a neuron fiber where '$r_a\Delta x$' represents the axial resistance to signal flow inside the nerve fiber due to axoplasm, and '$c_m\Delta x$' represents the membrane capacitance that characterizes the neuron fiber's thin lipid bilayer, 'r_m' is the specific resistance of axoplasm, and 'c_m' is the specific lipid membrane capacitance per unit length. The 'black box' in Figure3-1a can be represented as a HH membrane in case of an active membrane or a leakage conductance, as shown in Figure3-1b. The 'black box' represents the

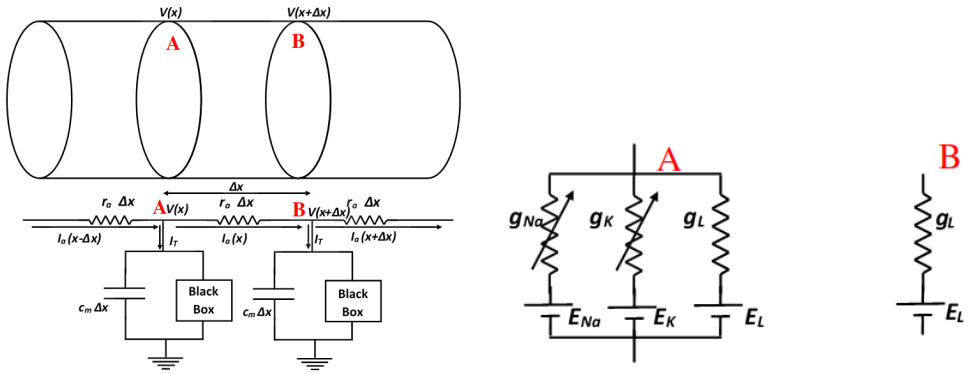

(a) **(b)**

Figure 3-1: Cable representation of a differential length of neuron fiber and membrane representation of active and passive fiber **(a)** Cable model equivalent circuit for a neuron fiber over a small length (Δx) of neuron fiber, **(b)** Black box representation from Figure3-1a with **A** representing electical circuit equivalent of a HH active membrane and **B** represents electical circuit equivalent of a passive membrane model.

localized membrane behavior depending on localized ion channel dynamics. As shown in Figure3-1b, 'A' is the electrical depiction of the active HH membrane, whereas 'B' is the electrical circuit equivalent of a passive membrane. Electrical parameters 'g_{Na}', 'g_k' and 'g_L' in Figure3-1b are the conductances due to $Na^{+}ion$ channels, $K^{+}ion$ channels and leakage ion channels respectively and 'E_{Na}', 'E_K' and 'E_L' are the equilibrium potential for $Na^{+}ions$, $K^{+}ions$ and leakage ions respectively.

3.3.1 Membrane Dynamics

Considering the cable circuit equivalent of a nerve fiber model for a infinitesimally small length of the fiber, Kirchhoff's circuit equation between two points 'A' and 'B', as shown in Figure3-1a can be summarized as

$$\frac{V(x+\Delta x)-V(x)}{\Delta x} = -I_a r_a \tag{3.1}$$

$$\frac{I_a(x-\Delta x)-I_a(x)}{\Delta x} = I_T \tag{3.2}$$

For a diferential length of fiber as $\Delta x \to 0$, equation 3.1 can be rewritten as

$$\lim_{\Delta x \to 0} \frac{V(x - \Delta x) - V(x)}{\Delta x} = -I_a r_a \tag{3.3}$$

$$\lim_{\Delta x \to 0} \frac{I_a(x - \Delta x) - I_a(x)}{\Delta x} = I_T \tag{3.4}$$

$$\frac{dV}{dx} = -I_a r_a \tag{3.5}$$

$$\frac{dI_a}{dx} = I_T \tag{3.6}$$

where I_T is the transmembrane current that flows perpendicular to the surface of the nerve fiber and can be mathematically modeled as

$$I_T = I_c + I_{ionic} \tag{3.7}$$

where 'I_c' denotes the current flowing across the capacitor and 'I_{ionic}' is the ionic current flowing across the membrane due to localize ion channel dynamics.

3.3.1.1 Active Membrane

As shown in Figure3-2, the active membrane can be modeled as an analogous electrical circuit, sometimes known as the HH [38, 39] membrane model or the conductance membrane model. In the HH model, the lipid bi-layer thickness separating the endoplasm from the exoplasm during axial ionic mobility works as a capacitance, whereas three variable conductances in parallel portray the voltage-controlled AICs corresponding to Na^+, K^+, and Cl^- ions. The voltage-controlled ion channels that enable and control ion exchange across the membrane are illustrated by the variable conductance 'g_{Na}', 'g_K', and 'g_L'.

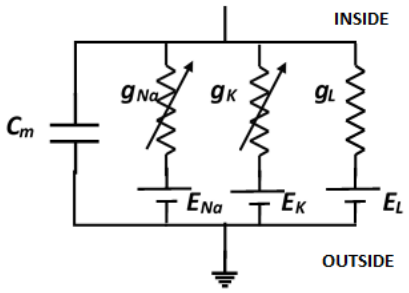

Figure 3-2: Active membrane dynamics of HH neuron.

The transmembrane current (I_T) dynamics in Figure3-2, due to the

voltage-controlled ion channels, can be mathematically described as

$$I_T = I_c + I_{Na} + I_K + I_L \tag{3.8}$$

where 'I_c' is the capacitive current due to electrostatic force across the membrane, 'I_{Na}' is the current due to Na^+ ion mobility across the membrane, 'I_K' is the current due to K^+ ion mobility across the membrane and 'I_L' is the leakage current due to minority ions. Current due to Na^+ ion channels are controlled via four gates controlling the flow of Na^+ ions, namely three 'm' gate and one 'h' gate, whereas the K^+ ionic exchange across the membrane is controlled via four 'n' gates and the equation 3.8 can be rewritten as

$$I_T = c_m \frac{dV}{dt} + g_{Na} m^3 h (V - E_{Na}) + g_K n^4 (V - E_K) + g_L (V - E_L) \tag{3.9}$$

$$I_T = c_m \frac{dV}{dt} + G_{Na} (V - E_{Na}) + G_K (V - E_K) + G_L (V - E_L) \tag{3.10}$$

where 'c_m' is the membrane specific capacitance, 'g_{Na}' is the maximum possible Na^+ conductance of the membrane, 'g_K' is the maximum possible K^+ conductance of the membrane. The term '$g_{Na} m^3 h$' portrays total Na^+ ion channels facilitating ion transport and '$g_K n^4$' portrays total K^+ ion channels facilitating ion transport and the gating dynamics of AICs are given as

$$\frac{dm}{dt} = \alpha_m (V)(1 - m) - \beta_m (V) m \tag{3.11}$$

$$\frac{dn}{dt} = \alpha_n (V)(1 - n) - \beta_n (V) n \tag{3.12}$$

$$\frac{dm}{dt} = \alpha_h (V)(1 - h) - \beta_h (V) h \tag{3.13}$$

$$\alpha_m (V) = 0.1 \frac{V + 40}{1 - e^{-\frac{V+40}{10}}}, \tag{3.14}$$

$$\alpha_n (V) = 0.01 \frac{V + 55}{1 - e^{-\frac{V+55}{10}}}, \tag{3.15}$$

$$\alpha_h (V) = 0.07 e^{-\frac{V+65}{20}}, \tag{3.16}$$

$$\beta_m (V) = 4 e^{-\frac{V+65}{18}}, \tag{3.17}$$

$$\beta_n (V) = 0.125 e^{-\frac{V+65}{80}}, \tag{3.18}$$

$$\beta_h (V) = \frac{1}{1 + e^{-\frac{V+35}{10}}} \tag{3.19}$$

Shown in Figure3-3 are the active membrane dynamics showing evolution

of APs during nerve stimulation. Shown in Figure3-3b, Figure3-3c and Figure3-3d shows the limit cycle of voltage gated m, n and h gate during the evolution of the AP.

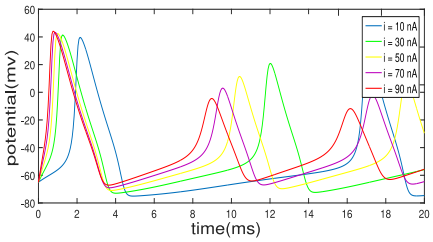

(a) Action potential in an active membrane for different injected current.

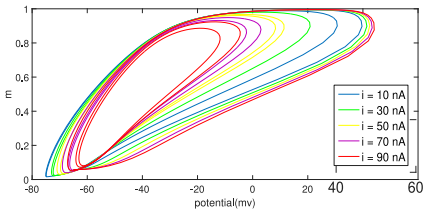

(b) Limit cycle of m gates due to different injected currents.

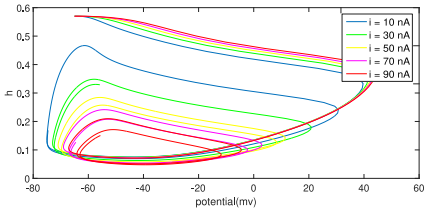

(c) Limit cycle of h gates due to different injected currents.

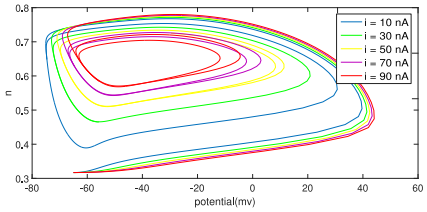

(d) Limit cycle of n gates due to different injected currents.

Figure 3-3: Action potential triggered by an HH type membrane due to injected stimulus and corresponding limit cycle of the Na^+ gates and K^+ gates due to membrane potential dynamics.

3.3.1.2 Passive Membrane

Shown in Figure3-4 is the passive cable representation of neuron fiber. The current and voltage equation for the passive cable equation is the same as shown in equation 3.3 and 3.5, whereas the major change in the membrane dynamics is seen in a cable passive membrane is due to the local ionic channel dynamics. In the case of a passive neuron fiber, localized ion channels governing the membrane dynamics is due to localized leakage channels, as shown in Figure3-4.

Thus the local membrane dynamics in a passive fiber can be summarized as

$$\frac{dV}{dx} = -I_a r_a \tag{3.20}$$

$$\frac{dI_a}{dx} = I_T \tag{3.21}$$

$$I_T = c_m \frac{dV}{dt} + g_L(V - E_L) \tag{3.22}$$

Differentiating equation 3.21 with respect to 'x' and substituting with the value

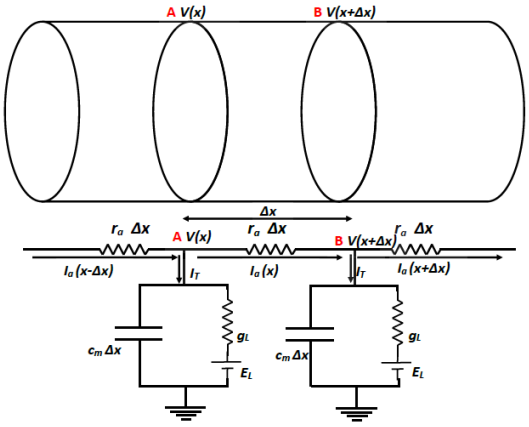

Figure 3-4: Passive cable representation of a differential length of neuron fiber.

of I_T in equation 3.22 the passive membrane. Shown in Figure3-5 is the transient response of a passive membrane for different initial conditions. Considering boundary conditions for a differential length of the equipotential fiber, the point process for membrane dynamics is described as

$$\frac{d^2V}{dx^2} = -r_a \left(c_m \frac{dV}{dt} + g_L(V - E_L) \right) \tag{3.23}$$

where the term $\frac{d^2V}{dx^2}$ describes the change in axially propagating potential as a consequence of the charge holding capacity of the membrane and diffusion of leakage ions across the nerve membrane. Equation 3.23 is the wave equation having multiple solutions depending on its initial and boundary conditions. $\frac{dV}{dx} = 0$ for an equipotential fiber, the equation (3.23) can be modeled to characterize the transient behavior for a short cable section. In order to understand the potential evolution along the length of the cable, equation 3.23 can be written as

$$\frac{d^2V}{dx^2} = -r_a g_L(V - E_L) \tag{3.24}$$

and the equivalent equation 3.24 is a wave equation with $r_a g_L$ as the dimensionless length constant for the cable, and the solution of the wave equation is a 'cosine' function. Similar to the evolution of the membrane equation 3.23 along the length of the fiber, the time evolution of the membrane equation 3.23 may be represented using appropriate boundary conditions. Time evolution of signals propagating in a neuronal fiber is of utmost interest in understanding of the basis of neuronal computation. A closed termination and an open termination have solutions to the cable equation, discussed in [150]. Shown in Figure3-5 is the transient response of a passive membrane for different initial conditions. Considering boundary conditions

for a differential length of the equipotential fiber, the point process for passive membrane dynamics can be described as

$$I_{inj} + c_m \frac{dV}{dt} + g_L(V - E_L) = 0 \tag{3.25}$$

where 'I_{inj}' is the forced input to the membrane. Shown in Figure3-5 is the passive fiber transients considering 'I_{inj}' to be 0 and the membrane settles from an initial membrane potential of $20mV$, $10mV$, $0mV$ and $-10mV$ to its resting state of membrane potential $-65mV$. When the passive membrane is stimulated with a constant forced input current, the resting potential of the membrane shifts either when the membrane is in a resting state or when the membrane settles from some initial membrane potential to its resting condition, as shown in Figure3-5b and Figure3-5c.

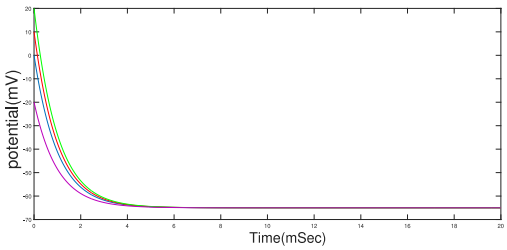

(a) Passive membrane transients for a cable of differential length while settling from different membrane potential to resting potential.

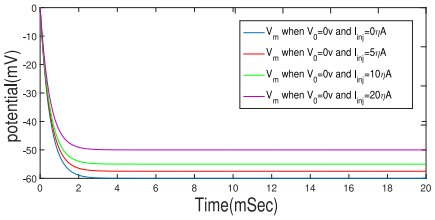

(b) Passive membrane transients for a cable of differential length while settling from different membrane potential to resting potential with current injected into the cable.

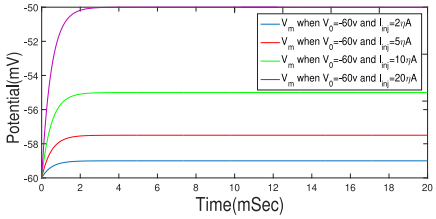

(c) Passive membrane transients for a cable of differential length at resting potential when stimulated with the external current.

Figure 3-5: Passive membrane transients from the cable model.

The point process description of the passive membrane model, shown in equation 3.25, can mimic membrane transients due to propagating current at that point. As a result, equation 3.25 can be modified to be able to calculate the propagating current to imitate the propagating action potential dynamics along with the passive nerve fiber. Considering current flow in a passive membrane, if

I_{AP} is the current at the inlet of the fiber, I_{axial} is the propagating current to the outlet of the fiber, and I_T is the transmembrane current due to membrane leakage, applying conservation of energy, the current equation can be rewritten as

$$I_{AP} = I_{axial} + I_T \tag{3.26}$$

With a longer cable, the only barrier to current flow is axial resistance, and current flow may be calculated as a function of the potential difference between the two sites of interest due to the linear behavior of the passive cable, with little leakage due to membrane leakage conductance. By replacing the cable parameters with lumped parameters, the equivalent circuit for a cable of uniform diameter D and length L can be characterized as shown in Figure3-6.

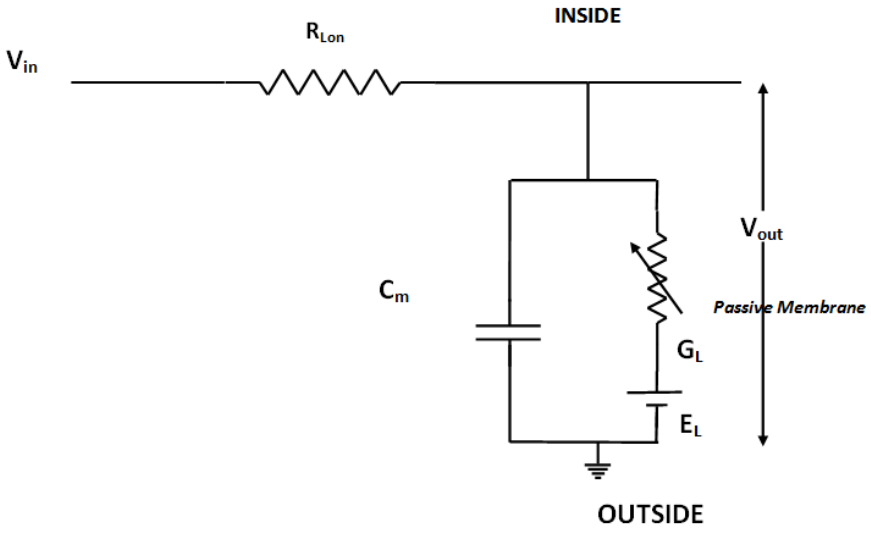

Figure 3-6: Equivalent discritized passive cable model representation.

The equivalent discretized passive model characteristic equation from Figure3-6 can be written as

$$\frac{V_{out} - V_{in}}{R_{Lon}} + C_m \frac{dV_{out}}{dt} + G_L \left(V_{out} - E_L\right) = 0 \tag{3.27}$$

where bulk membrane parameters in equation 3.27 for an uniform cable of length 'L', diameter 'D', specific axial resistance r_a and specific membrane parameters c_m, g_L can be expressed as

$$\begin{aligned} R_{Lon} &= \tfrac{4 r_a L}{\pi D^2} \\ G_L &= g_L \pi D L \\ C_m &= c_m \pi D L \end{aligned}$$

Figure3-7a shows propagation response surface plot at different locations of the passive fiber propagating throughout the length of the cable, whereas Figure3-7b simulates propagation response for discretized passive cables showing signal spread due to electrostatics of membrane capacitance. Figure3-7a suggests that due to axial resistance against volume conduction in the uniform fiber, signal propagation along the neural fibre is accommodated with an attenuation factor, and the attenuation factor affects propagation more in a longer fiber.

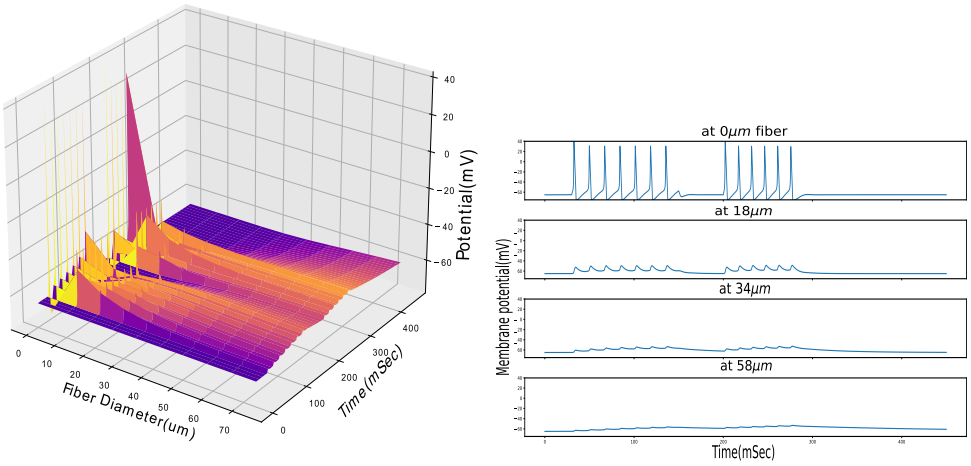

(a) **(b)**

Figure 3-7: Propagation response in fibers along the different lengths of the fiber **(a)** A surface plot from simulation model propagation response along the different lengths of the fiber of fiber diameter $5\mu m$ showing more propagation attenuation in fiber as the length of the fiber increases, **(b)** Propagation response plot for propagating action potential at different lengths of a passive fiber showing attenuation at different points along the length of the fiber. The response also shows an increase in signal spread due to increased electrostatic interaction due to membrane capacitance.

Figure3-7b shows the response of a signal propagating in a uniform fiber with a different diameter & constant length. Uniform fibers with smaller sizes show more attenuation than uniform fibers with higher diameters, according to simulation results in Figure3-7 and Figure3-8. Higher signal attenuation in uniform fibers with small diameters could be attributed to a reduction in ion mobility in a restricted region compared to uniform fibers with larger diameters.

Shown in Figure3-8 are the simulation responses of the signal propagating in nerve fiber of equal length and different diameters. Figure3-8a is a surface plot of signal propagation along with a fiber of various diameters. Figure3-8b shows the detailed time evolution of a signal propagating in equal length nerve fibers of varying diameters. The surface plot obtained from the simulation suggests that

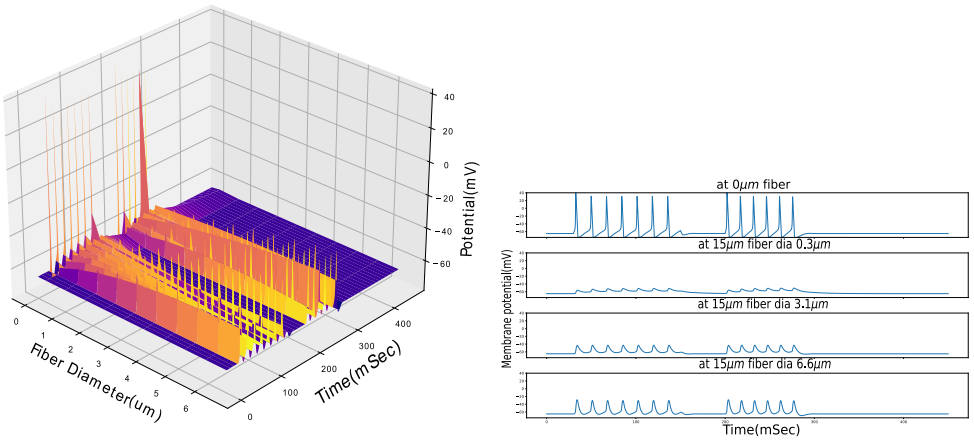

(a) **(b)**

Figure 3-8: Propagation response for fibers with different diameters. **(a)** A surface plot from simulation model propagation response along the different lengths of the fiber of fiber diameter $5\mu m$ showing more propagation attenuation in fiber as the length of the fiber increases and **(b)** Propagation response plot for propagating action potential at different lengths of a passive fiber showing attenuation at different points along the length of the fiber. The response also shows an increase in signal spread due to increased electrostatic interaction due to membrane capacitance.

attenuation is much more critical in a nerve cable with a small diameter than in a nerve fiber with a larger diameter. In larger diameter passive nerve fibers less attenuation may be due to increased ionic mobility capacity compared to smaller diameter nerve fibers.

3.3.2 Tapered and Flared Passive Fibers

An alteration in the shape of the dendritic arbor and its analogous electrical circuit could alter the overall response to a wide variety of input signals, from propagation delay to back-propagation in dendritic junctions. These effects have a substantial impact on the type of computation conducted by a cluster of dendrites on incoming signals, which may result in operations such as coherence detection, signal convolution, filtering, and so on. Dendrites at the distal end are narrow and serve primarily as input signal accumulators, whereas dendrites with larger diameters serve as filters. Aside from the mathematical formulation and comprehension of signal propagation in uniform passive nerve fiber, findings about fiber's diameter uniformity is limited. The majority of mathematical methodologies in use assume that the fiber diameter is coherent along its length. As a result, an attempt has been made to mathematically model and replicate flared/tapered passive neuron

fibers in order to comprehend their likely effects.

Shown in Figure3-9 is a $2D$ model of neuron fiber with a diameter D. For a differential length 'Δx' of the cable, the equivalent electrical circuit is shown with 'c_m', 'g_L' and 'r_a' as membrane's specific capacitance, specific leakage conductance and specific axial resistance respectively. '$V(x)$' and '$V(x+\Delta x)$' are the membrane potentials at A and B respectively seperated by a length of 'Δx', '$I_a(x+\Delta x)$' and '$I_a(x)$' are the axial current entering the node and leaving the node A respectively, 'I_T' is the transmembrane current.

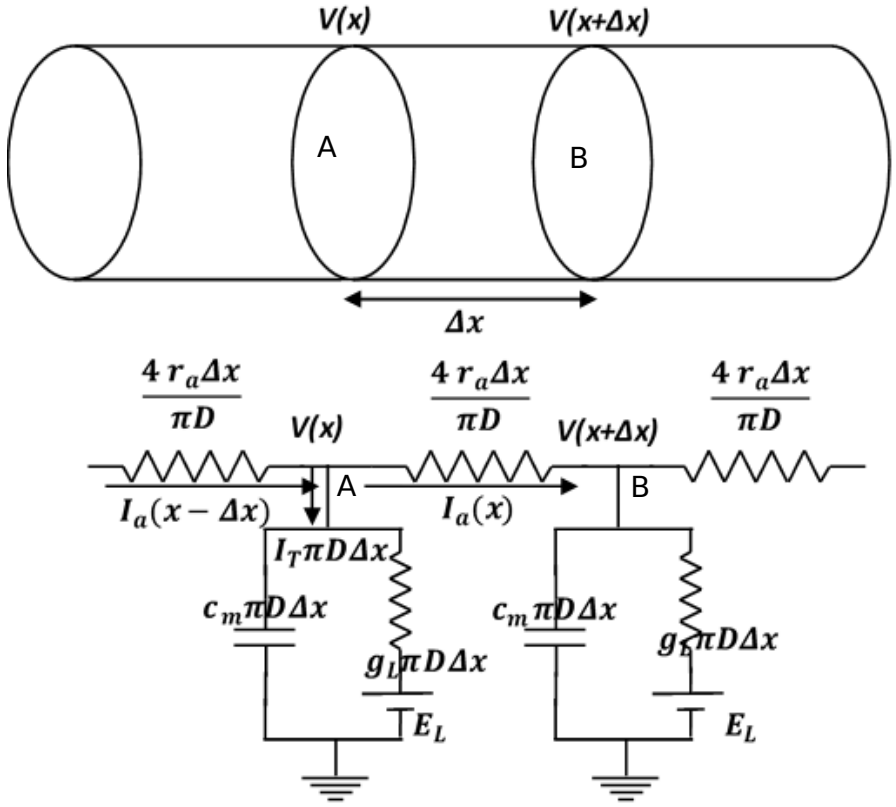

Figure 3-9: 2D equivalent of a cable fiber model.

3.3.2.1 Uniform 2D cable

When considering uniform passive 2D cable and comparing it to Figure3-9, the voltage and current equivalent equation for a differential length of uniform passive 2D fiber is given as

$$\frac{dV}{dx} = -\frac{4I_a r_a}{\pi D} \tag{3.28}$$

$$\frac{dI_a}{dx} = I_T \pi D \tag{3.29}$$

$$C_m \frac{dV}{dt} + G_L (V - E_L) = I_T \tag{3.30}$$

The equation 3.28, 3.29 and 3.30 are the equivalent equation where 'R_{Lon}', 'G_L' and 'C_m'are the aggregated parameters that are dependent functions of fiber length ('L') and diameter ('D'). In the case of a passive fiber, 'R_{lon}', 'G_L', and 'C_m' are all considered linear.

$$\begin{aligned} R_{lon}(L, D) &= \tfrac{4 r_a L}{\pi D^2} \\ G_L(L, D) &= g_L \pi D L \\ C_m(L, D) &= c_m \pi D L \end{aligned}$$

where 'r_a', 'g_L', and 'c_m' are characteristic parameters, 'L' is the length between the point of initiation and any point on the cable where the voltage transient is to be measured, and 'D' is the fiber diameter. The instantaneous membrane potential can be considered as equipotential if the propagating velocity is much greater than the differential length 'Δx', and the equation 3.30 can be summarized using the discretized cable equation and can be rewritten as

$$C_m \frac{dV}{dt} + G_L (V - E_L) = I_{prop} \tag{3.31}$$

such that $I_{prop} = \frac{V_{in} - V_{out}}{R_{Lon}}$ is the propagating current.

3.3.3 Tapered/flared 2D Cable

Comparing a tapered passive fiber with Figure3-9, for an infinitesimally small length of tapered passive fiber, Kirchhoff's circuit equation for the model are similar to equation 3.28, equation 3.29 and equation 3.30. Differentiating equation 3.28 with respect to 'x' we have

$$\frac{d^2V}{dx^2} = -\frac{4r_a}{\pi D}\left(\frac{dI_a}{dx} - \frac{2I_a}{D}\frac{dD}{dx}\right) \tag{3.32}$$

Replacing the expressions for $\frac{dI_a}{dx}$ from equation 3.29 in equation 3.32 the equation can be rewritten as

$$\frac{1}{R_{lon}}\frac{d^2V}{dx^2} = I_T\pi D\left(1 - \frac{2}{D}\frac{dD}{dx}\right) \tag{3.33}$$

where $\frac{1}{R_{lon}}\frac{d^2V}{dx^2}$ is equal to the propagating current in the discretized cable model, and '$I_T\pi D$' is the transmembrane current per unit length of membrane surface area. Thus the characteristic equation for the time evolution of signal propagating in a passive nerve membrane can be written as

$$C_m\frac{dv}{dt} + (V - E_L)\,G_L = I_{prop}\left(1 - \frac{2}{D}\frac{dD}{dx}\right) \tag{3.34}$$

such that $I_{prop} = \frac{V_{in} - V_{out}}{R_{Lon}}$ is the propagating current.

The signal propagation responses of a tapered/flared fiber are shown in Figure3-10, with the term $\frac{dD}{dx}$ in equation 3.34 as a tapering ratio along the length of the fiber. Figure3-10a and Figure3-10b shows the simulation responses for a flared fiber (diameter of the fiber increases along its length) and taper fiber (diameter of the fiber decreases along its length) respectively. The characteristics of signal propagation in a homogeneous cable are coherent with the propagation losses along the length of the fiber in the tapered fiber model, whereas the taper cable model generates some very interesting responses. Figure3-10a shows the propagation response of fibers with different flaring ratios, ranging from 0.1 to 6, where a flaring ratio ≈ 0 suggests a nearly uniform fiber. In a cable with a higher flaring ratio, the model predicts less signal attenuation than in a cable with a uniform diameter. Less signal attenuation in a flared fiber could be due to an increase in volume conduction and, as a result, a reduction in overall axial conduction resistance, which is entirely reasonable. When it comes to volume conduction, propagation attenuation is a function of ionic mobility and is proportional to the axial conductivity. Ionic mobility increases significantly as resistance decreases, and resistance changes are inversely proportional to the square of the fiber diameter, resulting in increased ionic mobility in fibers with larger diameters than fibers with smaller diameters.

Furthermore, Figure3-10b shows the propagation response of a tapered fiber with a tapering rate ranging from 0.1 to 6 and $tapering\ rate = -flaring\ rate$, which signifies that a tapering rate is a decrease in diameter along the length of the cable whereas a flaring rate is an increase in diameter along the length of the cable. As can be deduced from the preceding discussion, the ta-

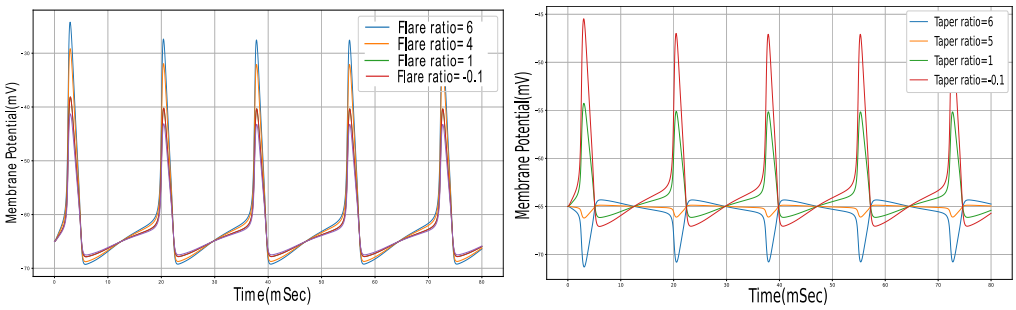

(a) **(b)**

Figure 3-10: Propagation response for tapered and flared fibers. **(a)**Simulation model propagation response along the different lengths of the fiber of initial fiber diameter $5\mu m$ with different flaring ratio showing more propagation attenuation in fiber as the length of the fiber increases, **(b)** Propagation response plot for propagating action potential at different lengths of a passive fiber with different tapering ratio showing attenuation at different points along the length of the fiber.

pering fiber is the polar opposite of the flaring fiber, in which the axial resistance increases along the length of the fiber and significantly attenuates the propagating signal along the length of the fiber. Under certain consequences, it is also been seen that the propagating signal is being reflected back, as in Figure3-10b with a tapering ratio $\frac{dD}{dx} = -5$ and $\frac{dD}{dx} = -6$. Such phenomena is because of the fiber's diameter shrinking, causing the signal to bounce back due to a discontinuity in the cable fiber. Discontinuity or mismatch in the cable fiber causes changes in the boundary condition, and the overall response is a reflection of the propagating signal at the discontinuity due to the law of conservation of electric charge.

In the case of cable with steady change such as $\frac{dD}{dx} \approx 0$ along the length of the fiber, the signal propagates steadily along the length of the fiber with steady attenuation to the propagating signal. Since the change in diameter of the fiber is ≈ 0 along the length, for a small section of fiber $Z_s \approx Z_L$, where Z_s is the source impedance, and Z_L is the load impedance. The reflection coefficient for the fiber is given as

$$\Gamma = \frac{Z_L - Z_s}{Z_L + Z_s} \tag{3.35}$$

In the case of a very low tapering ratio, the coefficient of reflection, $\Gamma \approx 0$ and $Z_L \approx Z_s$ and the reflection coefficient $\Gamma \approx 0$, whereas when the tapering rate changes dramatically $\frac{dD}{dx} >> 1$, the diameter of the fiber abruptly changes and the load impedance Z_L increases abruptly affecting the reflection coefficient thus resulting in signal reflection at the periphery of abrupt diameter change.

3.4 Cell-field Interaction and Inter-fiber Interference

Signal processing in neuronal fibers is just the tip of the iceberg. The neuronal learning systems and behaviors such as cognition, memory, and local function formation rely on a variety of neuronal attributes, including neuronal connectome specificity, complex neuronal morphologies, and localized ionic distribution. The cell-field interaction phenomenon and its possible role in the neural systems are two such attributes that have caught our attention. As a result of the development of methods such as EEG, MEG, as well as fMRI, which can capture local activities in the brain [158–160], neuronal electric local potential plays an important role in the mapping and study of neuronal network activity. Many studies on local field potentials (LFP)[161, 162], as well as cell-field interactions, have been conducted over the last few decades and successfully inter-linked LFPs to the causal function of AP. Either local interactions between synapses due to neurotransmitter mobility or ionic perturbations due to signal propagation in bundles of nerve fibers cause LFPs. Local field potential theories [163] are widely accepted because they are the effects of transmembrane currents [164, 165] and induction of an electric field (IEF) due to neuronal activity, and they have a strong relationship with network dynamics related to more complex functional responses such as cognition, memory, motor control, etc. [166, 167]. To demonstrate the significance of the transmembrane current and cell-field interaction, [168] investigates the effects, whereas software models such as "Electric Field Effects in Neural Networks" (ELFENN) in [169] are also proposed to model the ephaptic effects. In this proposed work, a cable approach is being used to model and simulate the phenomena of cell-field interaction. Extracellular to intracellular heterogeneity has been considered to determine the magnitude of effects on signal propagation in nearby fibers.

3.4.1 Bundled Nerve Fiber and Cable Model

A compartmental (passive) cable approach was used to model the local effects of a propagating signal in nearby fibers, with the membrane resistance controlling ionic channel leakage, the axial resistance controlling signal attenuation axially, and the extracellular cytoplasmic resistance between two fibers controlling the extracellular cytoplasmic resistance. The equivalent cable circuit depicted in Figure3-11 has been used to derive equivalent equations describing local membrane dynamics.

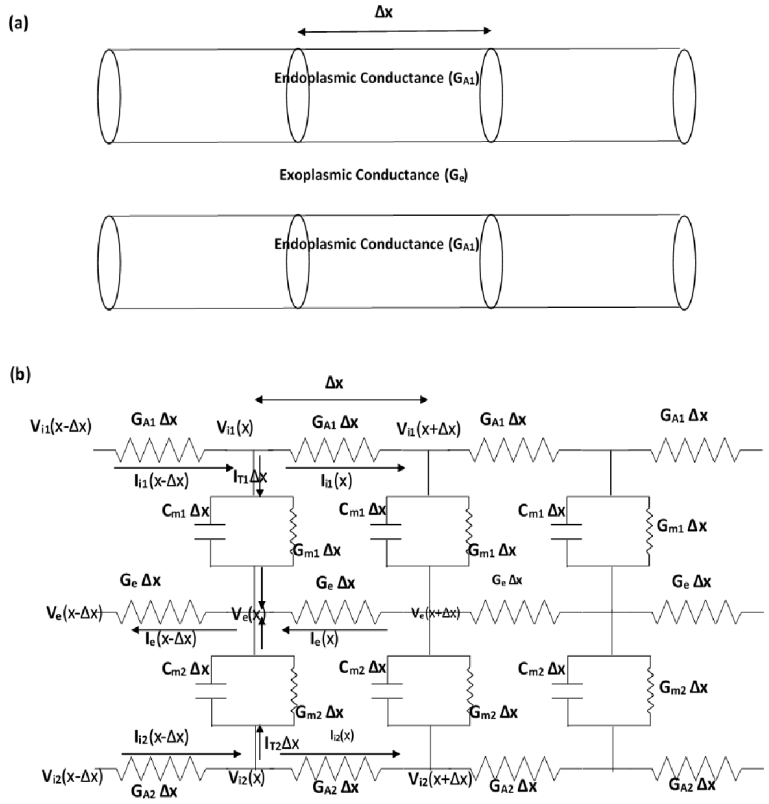

Figure 3-11: 2-fiber bundle and its equivalent cable representation.

Figure3-11 shows two cables that are perfectly parallel to one another, separated by ectoplasm, with axial resistances per unit length R_{a1}, R_{a2} due to endoplasm and R_e as extracellular resistance per unit length. The specific capacitance due to membrane thickness and membrane resistance due to leakage ion channels per unit length is C_{m1}, C_{m2} and R_{i1}, R_{i2}, respectively, for a passive fiber. The equivalent voltage and current equations over an infinitesimally small length of the fiber can be written as

$$\frac{dV_{i1}}{dx} = -I_{i1}R_{i1},\ \frac{dV_{i2}}{dx} = -I_{i2}R_{i2},\ \frac{dV_e}{dx} = I_eR_e \tag{3.36}$$

$$\frac{dI_{i1}}{dx} = I_{T1},\ \frac{dI_{i2}}{dx} = I_{T2},\ \frac{dI_e}{dx} = -(I_{T1} + I_{T2}) \tag{3.37}$$

Using V_e as the outside potential, V_{i1} and V_{i2} as the inside potentials for the two fibers, I_e is the extracellular current due to diffused ions from the nearby fiber and ionic redistribution due to the induced electric field, I_{i1} and I_{i2} are propagating current inside the nerve fiber due to mobile ions, I_{T1} and I_{T2} are

transmembrane current due to leakage ions across the membrane.

$$\frac{d^2V_{m1}}{dx^2} + R_{a1}I_{T1} + R_eI_{T2} + I_{inj_1} = 0 \tag{3.38}$$

$$\frac{d^2V_{m2}}{dx^2} + R_eI_{T1} + R_{a2}I_{T2} + I_{inj_2} = 0 \tag{3.39}$$

where 'I_{inj_1}' and 'I_{inj_2}' are currents that are injected when a fiber has synaptic connection or dendritic spines with synaptic contacts, 'R_e' in case of equation 3.38 is inter-fiber resistance from fiber-1 to fiber-2 and in case of equation 3.39 is the resistance from fiber-2 to fiber-1. Taking the fiber compartment to be isopotential over very small length of neuron fiber, the system of coupled equations 3.38 and 3.39 can be written as

$$\begin{bmatrix} C_{m1}R_{A1} & C_{m2}R_{e12} \\ C_{m1}R_{e21} & C_{m2}R_{A2} \end{bmatrix} \begin{bmatrix} \frac{dV_{m1}}{dt} \\ \frac{dV_{m2}}{dt} \end{bmatrix} = - \begin{bmatrix} R_{A1} & R_{e21} \\ R_{e12} & R_{A2} \end{bmatrix} \begin{bmatrix} I_{ion_1} \\ I_{ion_2} \end{bmatrix} + \begin{bmatrix} I_{inj_1} \\ I_{inj_2} \end{bmatrix} \tag{3.40}$$

where $R_{A1} = R_{a1} + R_e$ and $R_{A2} = R_{a2} + R_e$ are the cumulative axial resistance due to cytoplasm and R_{e12}, R_{e21} are the cross-coupled resistances of one fiber to the other and the equation is of the form

$$AX = BY + \phi \tag{3.41}$$

where A, B are the coupling matrices and ϕ is the forced inputs to the coupled fiber system and the solutions for $\frac{dV_x}{dt}$ can be given as

$$X = A^{-1}BY + A^{-1}\phi \tag{3.42}$$

The propagating current from the site of generation to the site of recording can be estimated by including diffusion losses and axial flow losses in the event of interference caused by fiber coupling further away from the site of action potential generation. An equivalent fiber of diameter D and length l for particular fiber compartment of specific membrane capacitance c_m, axial resistance r_a and membrane resistance r_{leak} can be represented in terms of bulk axial resistances R_{Ax} in series with parallel configuration of membrane capacitance C_x and leakage

membrane resistance R_{leak} and inter-fiber resistance R_{exy} which are selected from the ranges of biological values discussed in [170] [11] and described as

$$\begin{aligned} R_{Ax} &= \frac{4r_a l}{\pi D^2} \\ R_{exy} &= \frac{4r_e l_{xy}}{\pi D^2} \\ C_x &= c_m \pi D l \\ R_{leak} &= \frac{r_{leak}}{\pi D l} \end{aligned}$$

The inter-dendritic conductance and resistances in radially invariant and and collective branch convergence dendritic bundled fiber [171, 172], and the inter-dendritic spacing in dendritic bundled fiber is radially invariant [171]. As stated in [170], the effects of extracellular conductivity and generated electric field were previously disregarded. To better understand the impacts of signal transmission in inhomogeneous cytoplasmic conductivity media, the effects of signal propagation in such media have been attempted to be incorporated into a multi-fiber interaction model. In equation 3.43, R_{Ax} is the axial resistance for *fiber-x* against signal propagation due to ionic mobility in confined space inside the fiber, R_{exy} is resistance against ion mobility outside fiber directed from *fiber-x* towards *fiber-y* due to diffusion of leakage ions as well as ionic reconfiguration due to induced electric field within the vicinity, C_x is the total capacitance over the length of the fiber interaction region, and R_{leak} is the leakage resistance over the same, due to volume conductivity of mobile ions and induced electric field. This simple model can be easily converted to an n-fiber model under identical consideration, and the analogous equation can be expressed as

$$\begin{bmatrix} C_{m1}R_{A1} & C_{m2}R_{e12} & \dots & C_{mn}R_{e1n} \\ C_{m1}R_{e21} & C_{m2}R_{A2} & \dots & C_{mn}R_{e2n} \\ \vdots & \vdots & \ddots & \vdots \\ C_{m1}R_{en1} & C_{m2}R_{en2} & \dots & C_{mn}R_{An} \end{bmatrix} \begin{bmatrix} \frac{dV_{m1}}{dt} \\ \frac{dV_{m2}}{dt} \\ \vdots \\ \frac{dV_{mn}}{dt} \end{bmatrix} =$$

$$\begin{bmatrix} R_{A1} & R_{e21} & \dots & R_{en1} \\ R_{e12} & R_{A2} & \dots & R_{en2} \\ \vdots & \vdots & \ddots & \vdots \\ R_{e1n} & R_{e2n} & \dots & R_{An} \end{bmatrix} \begin{bmatrix} I_{ionic_1} \\ I_{ionic_2} \\ \vdots \\ I_{ionic_n} \end{bmatrix} + \begin{bmatrix} I_{inj_1} \\ I_{inj_2} \\ \vdots \\ I_{inj_n} \end{bmatrix} \tag{3.43}$$

The respective coupling resistances taken into account for the simulation of the 2-fiber interference model with the same diameter under various circumstances are presented in Figure3-12 and corresponding responses in Figure3-13. The two fibers in the coupling matrix B_2 have the same diameter of $4.2\mu m$, and perfectly aligned in parallel over a short length of $5\mu m$, with identical axial resistances. When fibers are interference-free, their inter-fiber resistances are equivalent and resemble those of a reciprocal network. Contrarily, when the coupling matrix $B4$ is taken into account, the axial resistances remain constant and the fibers have the same diameter, but the inter-fiber resistances increase when the fibers are packed closely. This increase in resistance is brought about by a reduction in the spatial mobility of ions. Small hyper- or depolarized deflections in one fiber relative to corresponding transients in the other are caused by the high resistance between the two fibers, which causes the majority of mobile ions to disperse fast and very few ions to interact.

$$B_1 = \begin{bmatrix} 15 & 7 \\ 4 & 15 \end{bmatrix} \quad B_2 = \begin{bmatrix} 15 & 4 \\ 4 & 15 \end{bmatrix} \quad B_3 = \begin{bmatrix} 15 & 4 \\ 7 & 15 \end{bmatrix} B_4 = \begin{bmatrix} 15 & 150 \\ 170 & 15 \end{bmatrix}$$

Figure 3-12: Some unique coupling matrices for a 2-fiber interaction model to simulate interference effects.

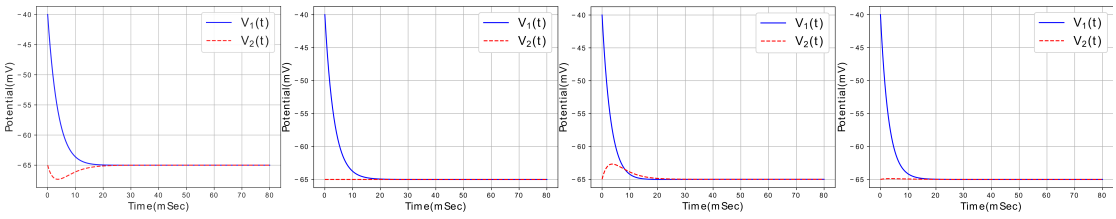

Figure 3-13: 2-fiber bundle transient response caused by various coupling matrices shown in Figure.3-12. Transients caused by coupling matrix B_1, B_2, B_3, and B_4 for a two-fiber interaction system, demonstrating coupling parameters capable of hyper-polarizing, depolarizing, and interference-free response in nearby fiber as one fiber settles to resting potential 65 mV from an initial membrane potential 0 mV.

Under similar circumstances, when the two fibers of same diameter are aligned with slight orientation mismatch as given in matrices B_1 and B_3 results in inter-fiber interaction. In coupling matrix, B_1, inter-fiber resistance from fiber-2 to fiber-1 is high as compared to the inter-fiber resistance from fiber-1 to fiber-2 leading to ionic mobility directed from fiber-1 to fiber-2 resulting in an instantaneous dip in membrane potential of fiber-2 due to increased ionic gradient outside of membrane with respect to the inside of the fiber and vice-versa in case of coupling matrix B_3.

$$B_1 = \begin{bmatrix} 15 & 3 & 0 \\ 11 & 15 & 11 \\ 0 & 11 & 15 \end{bmatrix} \quad B_2 = \begin{bmatrix} 15 & 3 & 0 \\ 3 & 15 & 3 \\ 0 & 3 & 15 \end{bmatrix}$$

$$B_3 = \begin{bmatrix} 15 & 12 & 0 \\ 7 & 15 & 4 \\ 0 & 13 & 15 \end{bmatrix} \quad B_4 = \begin{bmatrix} 15 & 0.002 & 0 \\ 0.004 & 15 & 0.005 \\ 0 & 0.0025 & 15 \end{bmatrix}$$

Figure 3-14: Different coupling matrices for the 3-fiber model in mode 2 to simulate interference effects.

Figure3-14 shows different coupling matrices for a 3-fiber system of neuronal fiber arranged linearly such that the fiber-1 has no direct interaction with fiber-3. The matrix B_2 and B_4 shows a configuration for interference-free coupling such that the system of coupled fiber are reciprocal in nature in the case of the matrix B_2 whereas the matrix B_4 suggests the three fibers being well separated such that the inter-fiber cytoplasm acts as a current sink and prevents active interaction between the three fibers. In contrast, the matrix B_2 and B_3 are calculated considering orientation mismatch in fiber-2 that shows expected transients due to the induced electric field during signal propagation, but at the same time, response in Figure3-15 infer that the induced electric field could influence the membrane potential of another fiber which is indirectly associated to the system. In the 3-fiber model shown in Figure3-15, similar depolarizing as well as hyper-polarizing effects [173] [174] [175] [176] can be seen. Apart from depolarizing and hyper-polarizing effects, synchronous sub-threshold oscillations in Figure3-17 is also generated due to inter-fiber interference with particular coupling parameters as discussed in [177] [178].

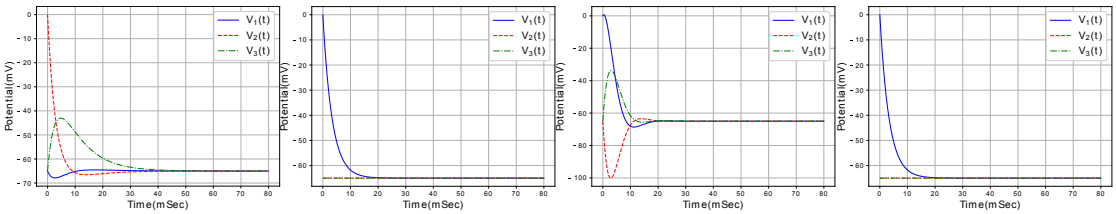

Figure 3-15: 3-fiber bundle transients due to different coupling matrices given in Figure3-14. Transients due to coupling matrix B_1, B_2, B_3 and B_4 for a 3-fiber interaction system showing coupling parameters capable of hyperpolarizing, depolarizing and interference free response in nearby fiber while one fiber settles to resting potential of $-65\ mV$ from an initial membrane potential of $0\ mV$.

Figure3-16 shows different coupling matrices for 3-fiber mode-1 system of neuronal fiber arrangements. The matrix B_1 shows a configuration for interference-

free coupling such that the system of coupled fiber forms a reciprocal network, and the system is free from interference due to signal propagation, as can be seen in Figure3-17. In the case of matrix B_3, three fibers with different diameter $4.2\mu m$, $4.4\mu m$ and $5.8\mu m$ have been used with each fiber aligned with some orientation mismatch. Fine inter-fiber separation facilitating good ionic mobility and at the same time doesn't allow quick dispersion of ions. When this system is triggered, the induced electric field between the three fibers traps some charges within their intersecting region of interaction and produces damped oscillations as the trapped charges start swaying within the overlapping field and delaying the overall settling time of the system.

$$B_1 = \begin{bmatrix} 15 & 7 & 7 \\ 7 & 15 & 7 \\ 7 & 7 & 15 \end{bmatrix} \quad B_2 = \begin{bmatrix} 15 & 4 & 4 \\ 10 & 15 & 11 \\ 11 & 5 & 15 \end{bmatrix} \quad B_3 = \begin{bmatrix} 15 & 6 & 9 \\ 7 & 14 & 5 \\ 5 & 12 & 8 \end{bmatrix}$$

Figure 3-16: Different coupling matrices for the 3-fiber model are arranged in a triangular pattern to simulate interference effects.

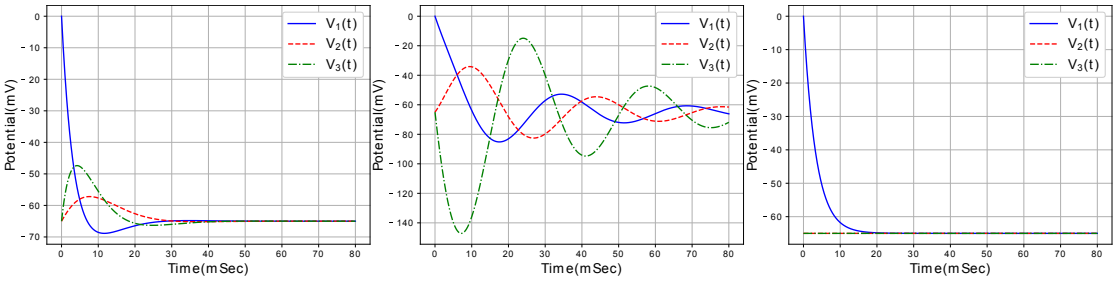

Figure 3-17: 3-fiber bundle transients due to different coupling matrices given in Figure3-16. Transients due to coupling matrix B_1, B_2 and B_3 for 3-fiber transients showing coupling parameters capable of transmission without signal interference on the other fibers while one fiber settles to resting potential of $-65\ mV$ from an initial membrane potential of $0\ mV$ in 3 fiber arrange in a triangular pattern.

3.5 Summary and Future Remarks

The linear and nonlinear characteristics of a nerve fiber are described by the passive and active models of nerve membrane. The active and passive models derived from the cable model could be easily applied to both linear and nonlinear systems. By cascading such systems in series or parallel as per requirement, several of the most complicated structures of neuronal assemblies, as well as dendritic arbors with localized active channels, can be simulated. The passive membrane model can be used to investigate filtering properties such as noise suppression, low pass

filtering, bandwidth tuning, and signal propagation characteristics such as propagation delays, as well as their roles in signal processing in neurons, which could be very useful in efficient modeling of complex neuronal architectures. Signal attenuation and propagation delay may play a role in neuronal assembly function formation. Aside from signal attenuation and delay, successful information transmission with minimal loss is desired for accurate signal interpretation. As a result, a thorough understanding of the transmission process and its dependence on the shape and length of the fiber is required. The tapered fiber model and simulation shows that a flared fiber transmits signals more efficiently and with less attenuation than a tapered and uniform counterpart, which could be one of the most likely scenarios as signal permeates from dendrites to the cell body. A flared fiber model, on the other hand, suggests higher attenuation and limits the amount of current propagating through the fiber; such a system might be plausible in the case of inter-neuron communication to limit the amount of current delivered to subsequent neurons in order to protect neurons from damage caused by high currents. Furthermore, the tapered fiber model can be used to simulate neuron fiber injury, which causes signal reflection along with the fiber, possibly leading to neuron fiber damage due to over current transmission caused by signal reflection and standing waves in the injured fiber. On a similar note, cell-field interaction might very well play a key role in defining the importance of neuron fiber interaction in the formation of complex structure-function relationships corresponding to neuronal structure arrangement in precise information, as discussed in the literature. As discussed in literature [173] [174] [176] [175], simulations from the inter-fiber interference model in a bundled fiber system without myelin show interference results. The model also shows that, depending on the coupling specifications, stimulating a fiber within a bundled fiber system can depolarize as well as hyper-polarize other fibers. The model shows that interference-free transport is also possible if the fibers are spaced far enough apart or if the bundled fiber system is reciprocal, which can be described using fiber coupling parameters. The proposed model is heavily influenced by morphogenesis and the effects of local or non-local collective signals on local signal processing. It can also be used to understand the underlying biological mechanism of pattern recognition, classification, and learning as possible functions of fiber coupling specifications as well as morphological parameters, which could lead to an increased learning activity.